JOURNAL OF MATERIALS SCIENCE **38** (2003) 1765–1771

Lamb wave evaluation and localization of transverse cracks in cross-ply laminates

N. TOYAMA, T. OKABE*
Smart Structure Research Center, National Institute of Advanced Industrial Science and Technology (AIST), 1-1-1 Umezono, Tsukuba, Ibaraki 305-8568, Japan
E-mail: toyama-n@aist.go.jp

N. TAKEDA
Department of Advanced Energy, Graduate School of Frontier Sciences, The University of Tokyo, 4-6-1 Komaba, Meguro-ku, Tokyo 153-8904, Japan

This paper investigates the effect of transverse cracks on the S_0 mode velocity in GFRP and CFRP cross-ply laminates, and proposes a new AE source location method that considers the change in the S_0 mode velocity due to the transverse cracks. We found experimentally that the stiffness and the velocity decreased as the transverse crack density increased. Analytical predictions deduced from the combination of the complete parabolic shear-lag analysis, the classical plate theory and the laminated plate theory are in good agreement with the experimental results. Utilizing this relationship between the velocity and the mechanical damage, we located AE sources of transverse cracks in cross-ply laminates with the calculated *in situ* velocity. We were able to show that highly accurate source location requires the reduction of the *in situ* value of the velocity. The present method is simple but quantitative and useful in health-monitoring for detecting and localizing the damage in composite structures.

1. Introduction

Composite laminates are advantageous as structural components for aircraft and spacecraft because of their high specific strength and stiffness. In recent years, structural health monitoring has become the focus of attention in order to reduce maintenance cost and improve safety and reliability. When laminates are subjected to mechanical and thermo-mechanical loading, damage such as transverse cracking, delamination and fiber breakage results and may cause significant loss of strength or stiffness.

Of the above damage, transverse cracking, one of the most frequently encountered types of damage in composite laminates, can be detrimental to the stiffness and dimensional stability. One serious concern is that transverse cracks may become leak paths when composite laminates are applied as structural components for liquid fuel tanks. Therefore, analyzing the effect of the crack density on the stiffness reduction [1–6] and monitoring the cracks nondestructively, for example, with acoustic emission [7–10] and optical fiber sensors [11–13] have become subjects of considerable interest.

Among the various techniques available, ultrasonic Lamb waves offer a convenient approach for evaluating the composite laminates. The Lamb wave velocity depends on the in-plane stiffness of the laminate, so some authors evaluated fatigue damage [14], thermal damage [14, 15] and fiber volume fraction [16] by measuring the velocity. Studies have been conducted on monitoring transverse cracks that reduce stiffness [14, 17–19]. The acoustic emission method is also useful due to its sensitivity and source location accuracy for damage and impacts [20–23]. To accurately locate AE sources, the *in situ* wave velocity should be used in the calculation if the laminate is damaged. Active sensing of measuring the *in situ* Lamb wave velocity and passive sensing of detecting acoustic emission must therefore be combined to monitor the transverse cracks accurately. However, as far as we know, there have been no studies considering the change in the wave velocity with the AE source location.

In the present study, we measured the stiffness and the velocity of the lowest order symmetric (S_0) mode for GFRP and CFRP cross-ply laminates with various transverse crack densities. The reduction of the stiffness and the velocity as a function of the crack density were calculated analytically. The predicted values were then compared with the experimental results. Furthermore, linear AE sources were located in the damaged specimens, and the effect of the change in the velocity on the accuracy of the source location was investigated.

2. Specimen preparation

The materials studied were E-glass/epoxy (GFRP) and T300/epoxy (CFRP) with stacking sequences of

*Author to whom all correspondence should be addressed.

TABLE I Properties of unidirectional GFRP and CFRP laminates

Property	GFRP	CFRP
Longitudinal Young's modulus, E_{11} (GPa)	38.1	116.9
Transverse Young's modulus, E_{22} (GPa)	10.51	8.59
Longitudinal shear modulus, G_{12} (GPa)	4.03	5.8
Transverse shear modulus, G_{23} (GPa)	3.10	3.75
Poisson's ratio, ν_{12}	0.32	0.33
Ply thickness (mm)	0.1	0.2
Density, ρ (kg/m^3)	1910	1520

$[0_2/90_{12}/0_2]$ and $[0/90_8/0]$. These composite plates were fabricated with unidirectional prepregs by a hot-press machine in accordance with the manufactures' recommended processes. Tensile coupons (200 mm × 10 mm) for each laminate were cut from the plates (300 mm × 300 mm). The GFRP specimens were 1.6 mm thick, and the CFRP specimens, 2.0 mm. The measured material properties of the unidirectional GFRP and CFRP laminates are shown in Table I. These values were used to calculate the stiffness reduction due to the transverse cracks and the S_0 mode velocity of the laminates.

3. Theoretical background

In this section, we will briefly introduce the analytical procedure for predicting the S_0 mode velocity and the quantitative relationship between the stiffness and the transverse crack density.

At frequencies below 1 MHz, only the lowest order S_0 mode and the lowest order A_0 mode propagate for thin plates. In this region, the S_0 mode velocity is slightly dispersive, and the A_0 mode velocity is highly dispersive. The velocities of both modes are directly related to the properties of the material. Therefore, the stiffness of composite laminates can be evaluated by measuring the Lamb wave velocity. Here, the S_0 mode velocity has a higher dependence on the in-plane stiffness than the A_0 mode velocity. Only the solutions for the S_0 mode are treated here.

The velocity of the S_0 mode for the 0° direction of the laminate is expressed by the classical plate theory as [15]

$$V = \sqrt{\frac{A_{11}}{\rho h}} \tag{1}$$

where A_{11} is the in-plane stiffness for the entire plate, ρ is the density, and h is the thickness of the plate. A_{11} is defined by the laminated plate theory as [18]

$$A_{11} = \frac{E}{1 - \nu_{12}\nu_{21}} h \approx Eh \tag{2}$$

where E is Young's modulus of the laminate in the 0° direction, and ν_{12} and ν_{21} are the major and minor Poisson's ratios of the laminate.

Young's modulus of the cross-ply laminates with transverse cracks can be derived from a complete parabolic shear-lag analysis [5] that yields a fairly good approximation of the strain and stress distributions obtained by the finite element method. The Young's modulus reduction of the cross-ply laminates with equally distributed transverse cracks is expressed as

$$\frac{E_x}{E_x^0} = \left(1 + \frac{t_{90}}{t_0}\frac{E_{90}}{E_0}\frac{2t_{90}D}{\eta}\tanh\frac{\eta}{2t_{90}D}\right)^{-1} \tag{3}$$

where E_x and E_x^0 are the Young's moduli of the damaged and undamaged laminates, respectively. t_0 and t_{90} are the half thicknesses, and E_0 and E_{90} are the Young's moduli of the 0° layers and the 90° layers. D is the crack density, and η is the shear lag parameter [5].

The reduction of the S_0 mode velocity for the crack density D is derived using Equations 1–3 as

$$\frac{V}{V_0} = \sqrt{\frac{E_x}{E_x^0}} = \sqrt{\left(1 + \frac{t_{90}}{t_0}\frac{E_{90}}{E_0}\frac{2t_{90}D}{\eta}\tanh\frac{\eta}{2t_{90}D}\right)^{-1}} \tag{4}$$

where V and V_0 are the S_0 mode velocities for damaged and undamaged laminates, respectively. Thus, a quantitative relationship between the reduction of the S_0 mode velocity and the transverse crack density was obtained.

4. Measurement of the Lamb wave velocity

The experimental setup for measuring of the S_0 mode velocity is shown in Fig. 1. Two AE sensors (Fuji Ceramics, Model M304A) with a diameter of 4 mm were mounted on the plates via a coupling gel. The distances between the sensors L were set to 2.5, 5, 7.5

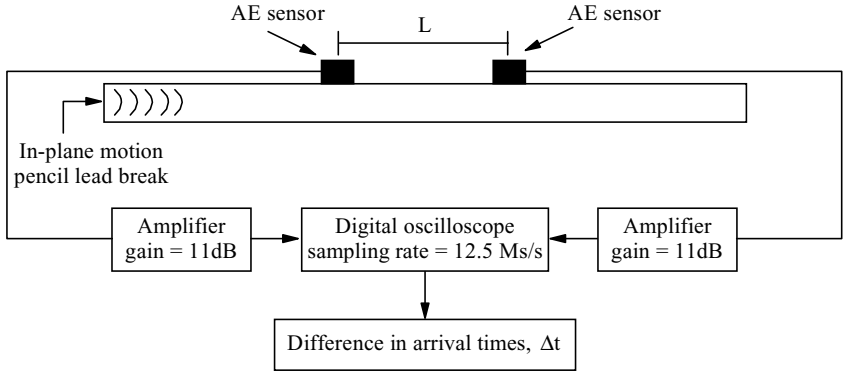

Figure 1 Experimental setup for the Lamb wave measurement.

TABLE II Experimental and theoretical S_0 mode velocities for GFRP and CFRP laminates

Meterial	Laminate	Experimental (m/s)	Theoretical (m/s)
GFRP	$[0_{16}]$	4685	4530
	$[90_{16}]$	2547	2379
	$[0_2/90_{12}/0_2]$	3196	3062
CFRP	$[0_8]$	8915	8805
	$[90_8]$	2663	2387
	$[0/90_8/0]$	4582	4479

and 10 cm. A pencil lead break was made on a longitudinal edge of the specimen (in-plane motion) to generate a high-amplitude Lamb wave in the S_0 mode. Detected signals were amplified (gain = 11 dB) and recorded using a digital oscilloscope at a sampling rate of 12.5 Ms/s. The arrival times of the S_0 mode at the two AE sensors were determined from a cursor-based phase-point matching method. Least-square fits from a plot of differences in arrival times and distances were performed to obtain the S_0 mode velocity of the laminates.

Table II shows the measured and predicted S_0 mode velocities for various GFRP and CFRP laminates. The measured S_0 mode velocities were in good agreement with the predicted ones in both materials. These results validate applying Equation 1 to predict the S_0 mode velocity of the laminates.

5. Effects of transverse cracks on the stiffness and the Lamb wave velocity

In this experiment, the effects of the transverse cracks on the stiffness and the S_0 mode velocity of the cross-ply laminates were investigated by using special specimen coupons.

5.1. Specimens and experimental setup

To obtain specimen coupons with the designed numbers and positions of transverse cracks, we introduced artificial flaws on the optional positions of the 90° layers at an edge of the specimen with a knife within a range of 50 mm. We chose 50 mm to be the same as the gauge length of the extensometer, as described below. The tensile load was then applied by a tensile machine until the transverse cracks were initiated and penetrated through the specimen width at all positions of the flaws. We confirmed that only transverse cracks were initiated (no delamination) before the final failure by microscopic observations. Using this technique, we were able to measure the stiffness and the S_0 mode velocity of the cross-ply laminates with optional transverse crack density.

The stiffness was measured by tensile tests. During the tests, the strain was measured by an extensometer with a gauge length of 50 mm. In order to measure the global strain between the cracked regions, we selected an extensometer, not strain gauges, which measure only the local strain. After measuring the stiffness, we removed the specimen from the tensile machine and measured the S_0 mode velocity with the same system as shown in Fig. 1. Unlike the case for undamaged laminates, we fixed the distance of the two sensors to 50 mm (same as the cracked regions). The S_0 mode velocity was calculated by dividing the distance between the sensors by the difference in the arrival times. After measuring the stiffness and S_0 mode velocity, we introduced additional artificial flaws to achieve higher crack density. We repeated these procedures several times and thus experimentally obtained the stiffness and the S_0 mode velocity as a function of transverse crack density.

5.2. Experimental and analytical results

The experimental results and predictions for variations of the stiffness for GFRP and CFRP laminates as a function of crack density are shown in Fig. 2. Three tensile coupons for each laminate were used to obtain these plots. As expected, the stiffness decreased as the crack density increased. The results deduced from the analytical model (Equation 3) agreed well with the experimental results, as reported by Berthelot *et al.* [5].

The experimental results and predictions for variations of the S_0 mode velocity for GFRP and CFRP as a function of crack density are shown in Fig. 3. The

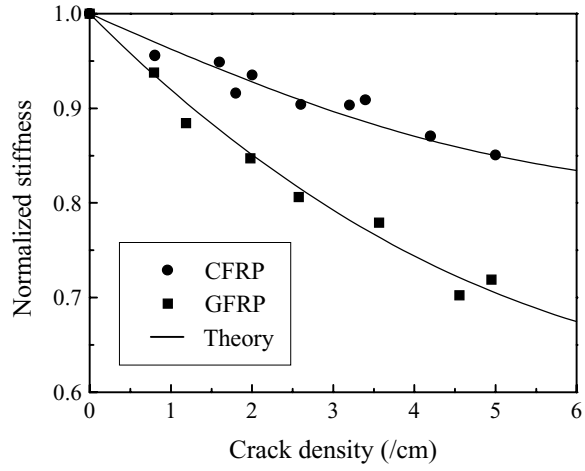

Figure 2 Experimental and theoretical normalized stiffness as a function of crack density for GFRP $[0_2/90_{12}/0_2]$ and CFRP $[0/90_8/0]$ laminates.

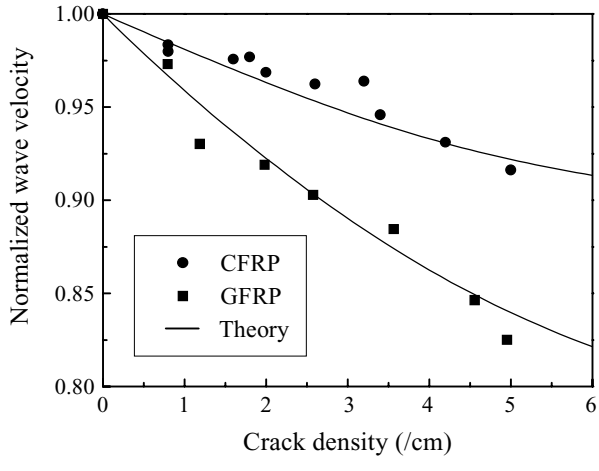

Figure 3 Experimental and theoretical normalized S_0 mode velocities as a function of crack density for GFRP $[0_2/90_{12}/0_2]$ and CFRP $[0/90_8/0]$ laminates.

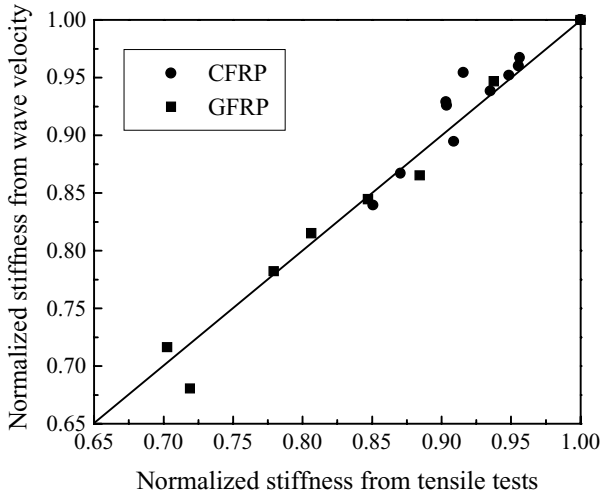

Figure 4 A comparison of the normalized stiffness from tensile tests versus calculated from the wave velocity.

predicted values deduced from Equation 4 are in good agreement with the experimental results. Furthermore, Fig. 4 depicts a comparison of the normalized stiffness from tensile tests versus calculated from the wave velocity. They agree well for both laminates and these results indicate that the S_0 mode propagates with the velocity expressed by Equation 1, even if the laminates are damaged. It should be noted that the number of the transverse cracks can be evaluated quantitatively by measuring the S_0 mode velocity. In this study, S_0 mode velocity measurement is demonstrated to be an excellent method of monitoring transverse cracks in composite laminates.

6. AE detection and localization of transverse cracks

Based on the knowledge in the former section, we calculated the *in situ* S_0 mode velocity and located the AE source with the *in situ* S_0 mode velocity on the transverse cracks.

6.1. Specimens and experimental setup

We first performed tensile tests on CFRP specimens with no artificial flaws. However, we observed fewer than five cracks along the gauge length before the final failure. The main purpose of this work is to evaluate the effect of the change in the S_0 mode due to the transverse cracks on the accuracy of the AE source location. We therefore introduced artificial flaws with intervals of about 2 mm between the AE sensors on the 90° layers of both GFRP and CFRP specimens to initiate more than 40 transverse cracks, which corresponded to about five cracks per centimeter for the transverse crack density.

The experimental setup for the AE measurement is shown in Fig. 5. Two AE sensors were mounted on the specimen via a coupling gel for linear source location. Each sensor was fastened mechanically by using metal fittings to prevent the sensors from splitting off due to the impacts of crack initiations. After confirming that all the transverse cracks initiated from the flaws, we aligned the outer edge of each sensor with the flawed edge of the specimen to improve the accuracy of the source location. The distances between the two sensors were set to 85 mm for both GFRP and CFRP specimens. The detected signals were amplified (gain = 11 dB) and recorded in a digital acoustic emission acquisition system (JT-TOSHI, DCM-140) at a sampling rate of 10 Ms/s.

When one AE event was detected during the tensile test, the load was stopped and the transverse crack and its location was examined in situ using an optical microscope with a x-z transition stage. The surface of the GFRP specimen was observed due to its transparency, and one polished edge of the CFRP specimen was observed. The load was then applied again and this procedure was repeated until more than 40 cracks had been initiated. Thus noise and AE signals due to the transverse cracks located outside the two sensors were eliminated, and one-to-one correspondences between the AE signals and transverse cracks between the sensors were obtained.

6.2. Time-frequency analysis of the Lamb wave due to transverse crack

Typical waveforms detected at the two sensors due to a transverse crack in the GFRP specimen are shown in Fig. 6. This crack corresponds the seventh crack located 71 mm from sensor 1 and 14 mm from sensor 2. The motion of the transverse crack face is parallel to the plane of the specimen (in-plane motion), so the AE waves contain a predominant S_0 mode. We performed time-frequency analysis using wavelet transform and the associated contour maps are shown in Fig. 6. The peak of the wavelet magnitude corresponds to the arrival time of the group velocity [21]. Because of the

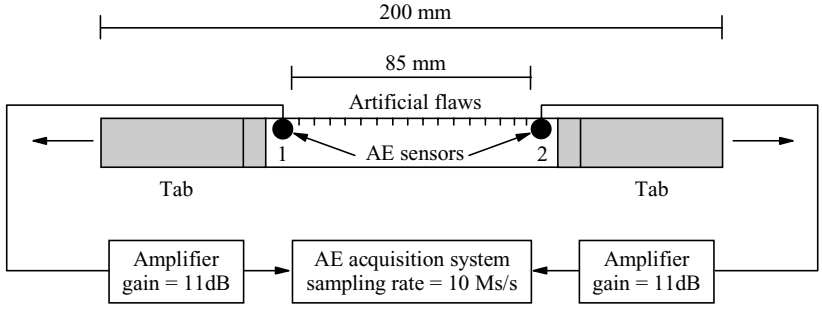

Figure 5 Experimental setup for the AE measurement.

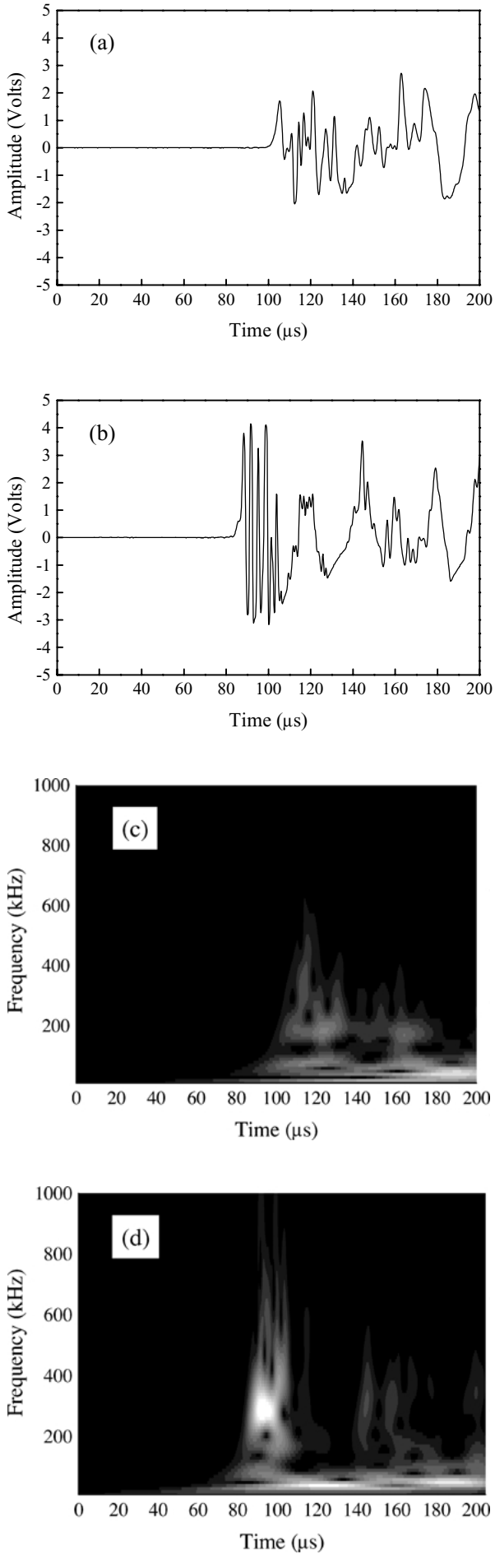

Figure 6 Waveforms detected at (a) sensor 1 and (b) sensor 2 due to a transverse crack and their wavelet contour maps: (c) sensor 1 and (d) sensor 2.

narrow width of the specimen coupon, many peaks corresponding to multiple reflections are observed. The peaks corresponding to the arrival times of the A_0 mode should be included in the contour maps. However, its magnitude is very small for the in-plane source, so it is difficult to distinguish the A_0 mode from the S_0 mode and its reflections.

6.3. Determining arrival time of S_0 mode and a new AE location method

From Fig. 6d, the first arrival time of the S_0 mode at sensor 2 can be estimated to be 90 μs, and the velocity showed little dispersion below 1 MHz. We also observed considerable attenuation of high frequency components in Fig. 6c. This attenuation caused difficulty in determining the arrival times of the S_0 mode from the wavelet peak, because high frequency components are used to distinguish the first peak from the second peak corresponding to the reflection. In the case of relatively low frequency components below 500 kHz, the first peak and the second peak were mixed. Thus, although it was possible to determine the arrival times by manually distinguishing the very small magnitude wavelet peak of the high frequency components, it was impossible to do so automatically. The first peaks of the detected AE waves were clear, and their amplitudes were high as shown in Fig. 6a and b, therefore, the conventional threshold method was adopted to automatically determine the arrival times of the S_0 mode.

The source location was calculated by

$$x = \frac{L - V\Delta t}{2} \tag{5}$$

where x is the distance from the edge of the sensor 1, L is the distance between the sensors (85 mm), V is the *in situ* velocity calculated by Equation 4, and Δt is the difference in arrival times at the two sensors.

The global crack density D is determined by

$$D = \frac{N_{\mathrm{AE}}}{L} \tag{6}$$

where N_{AE} is the number of AE events due to the transverse cracks between the sensors.

By using Equations 4–6, we could calculate the linear AE location with *in situ* S_0 mode velocity without measuring the *in situ* velocity.

6.4. AE source location results

Fig. 7 shows the locations on the GFRP specimen calculated using the *in situ* velocity (present method) and with constant initial velocity (conventional method) as compared to microscopic observations. The transverse cracks were first distributed mainly on the right side (sensor 2) of the specimen, then shifted toward the left side (sensor 1), and finally, the 40 cracks were distributed evenly with an interval of about 2 mm. The average errors of every 10 cracks for both methods are also shown in Fig. 7. As the number of cracks increased, the errors in the conventional method increased. The

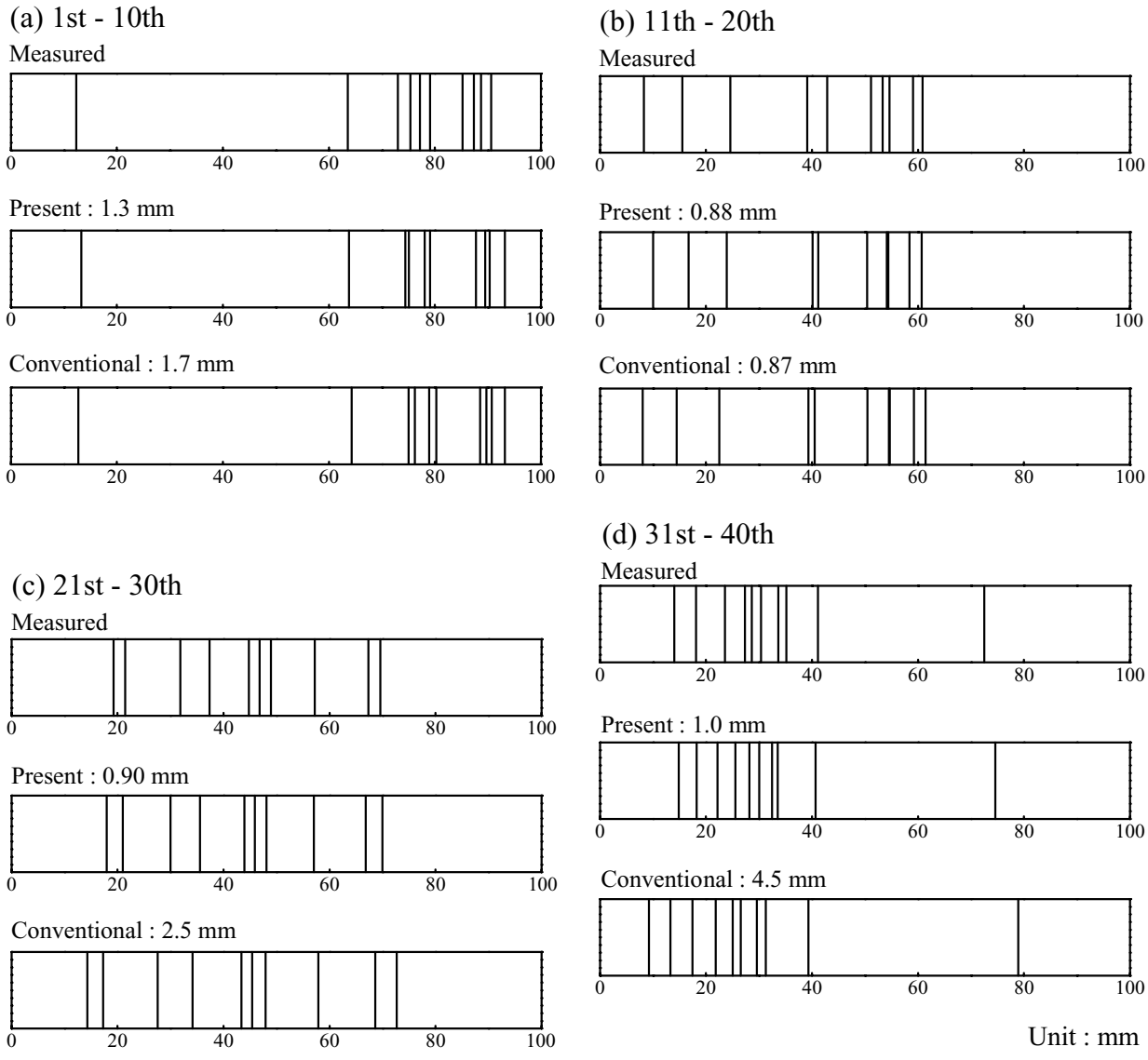

Figure 7 Source location results and average errors of every 10 cracks with the present and conventional methods on transverse cracks for GFRP specimen, (a) 1st–10th, (b) 11th–20th, (c) 21st–30th and (d) 31st–40th.

source locations for the last 10 cracks (Fig. 7d) obviously disagreed with the observation with an average error of 4.5 mm. In contrast, the errors remained small for all cracks in the present method, and location accuracies were drastically improved. As reported by Prosser *et al.* [8], the threshold method may induce location errors, especially for out-of-plane sources with low amplitude of S_0 mode due to attenuation. In this study, the objective sources were ideal in-plane sources with a high amplitude S_0 mode, so we obtained high accuracy in spite of the attenuation effects.

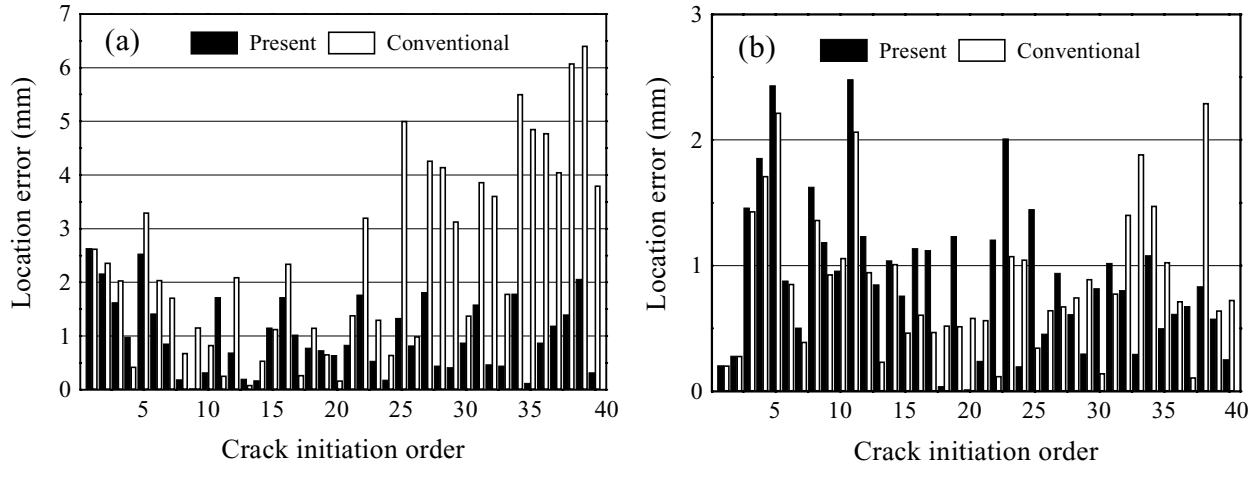

Figure 8 Source location errors for 40 cracks with the present and the conventional method: (a) GFRP specimen and (b) CFRP specimen.

Fig. 8 shows the location errors for the all cracks in GFRP and CFRP specimens. As shown in Fig. 8a, an obvious improvement in accuracies can be observed in the GFRP specimen. In the CFRP specimen, the average error of the 40 cracks was 0.90 mm for both the present and conventional methods. However, the average error of the last 10 cracks was 0.66 mm for the present method and 1.1 mm for the conventional method. A slight improvement in location accuracy was obtained in the last 10 cracks. On the whole, however, the effect of the reduction of the S_0 mode velocity on the location accuracy was small compared with the effects of the attenuation and errors in measurements including the real location of the sensors and the transverse cracks, and the S_0 mode velocity. Therefore, reasonably good accuracies were obtained using both methods.

In spite of the small specimen sizes, the effects of the reduction in S_0 mode velocity on the location accuracy were observed, especially in GFRP specimen. These results indicate that the *in situ* velocity must be used for inspecting large and/or considerably damaged laminates.

7. Conclusion

This study investigated the effects of transverse cracks on the velocity of the S_0 Lamb wave in GFRP $[0_2/90_{12}/0_2]$ and CFRP $[0/90_8/0]$ cross-ply laminates. A new AE source location method that considers the reduction of the wave velocity due to the transverse cracks was also proposed to improve the accuracy of the crack location.

The reduction of the stiffness and S_0 mode velocity were obtained experimentally as a function of the transverse crack density, and the results were in good agreement with the theoretical results deduced from the complete parabolic shear-lag analysis, classic laminate theory and classic plate theory. These results indicate that the S_0 mode velocity measurement is an excellent quantitative method of monitoring the transverse crack density in the composite laminates.

The AE sources were located with *in situ* S_0 mode velocity on the transverse cracks. For CFRP cross-ply laminates, the reduction of the S_0 mode velocity due to the transverse cracks was low, so good location accuracy was obtained for both conventional and present methods. However, for GFRP cross-ply laminates, AE source locations with the conventional method in the high crack density area obviously disagreed with the observation. In contrast, the errors remained small for all cracks in the present method, and location accuracy was drastically improved. These results indicate that the *in situ* velocity must be used for inspecting large and/or considerably damaged laminates.

References

1. K. W. GARRET and J. E. BAILEY, *J. Mater. Sci.* **12** (1977) 157.
2. H. FUKUNAGA, T.-W. CHOU, P. W. M. PETERS and K. SCHULTE, *J. Compos. Mater.* **18** (1984) 339.
3. S. G. LIM and C. S. HONG, *Compos. Sci. Technol.* **34** (1989) 145.
4. N. TAKEDA and S. OGIHARA, *ibid.* **52** (1994) 183.
5. J.-M. BERTHELOT, P. LEBLOND, A. EL. MAHI and J.-F. LE CORRE, *Composites* Part A **27A** (1996) 989.
6. J.-M. BERTHELOT, *J. Compos. Mater.* **31** (1997) 1780.
7. M. R. GORMAN and S. M. ZIOLA, *Ultrasonics* **29** (1991) 245.
8. W. H. PROSSER, K. E. JACKSON, S. KELLAS, B. T. SMITH, J. MCKEON and A. FRIEDMAN, *Mater. Eval.* **53** (1995) 1052.
9. M. SURGEON and M. WEVERS, *NDT&E Int.* **32** (1999) 311.
10. M. JOHNSON and P. GUDMUNDSON, *Compos. Sci. Technol.* **60** (2000) 2803.
11. Y. OKABE, S. YASHIRO, T. KOSAKA and N. TAKEDA, *Smart Mater. Struct.* **9** (2000) 832.
12. R. A. BADCOCK and G. F. FERNANDO, *ibid.* **4** (1995) 223.
13. D. C. LEE, J. J. LEE, I. B. KWON and D. C. SEO, *ibid.* **10** (2001) 285.
14. M. D. SEALE, B. T. SMITH and W. H. PROSSER, *J. Acoust. Soc. Amer.* **103** (1998) 2416.
15. M. D. SEALE and E. I. MADARAS, *J. Compos. Mater.* **34** (2000) 27.
16. M. D. SEALE, B. T. SMITH, W. H. PROSSER and J. N. ZALAMEDA, *J. Acoust. Soc. Amer.* **104** (1998) 1399.
17. B. TANG and E. G. HENNEKE II, *Mater. Eval.* **47** (1989) 928.
18. V. DAYAL and V. K. KINRA, *J. Acoust. Soc. Amer.* **89** (1991) 1590.
19. N. TOYAMA, T. OKABE, N. TAKEDA and T. KISHI, *J. Mater. Sci. Lett.* **21** (2002) 271.
20. N. TOYAMA, J.-H. KOO, R. OISHI, M. ENOKI and T. KISHI, *ibid.* **20** (2001) 1823.
21. H. JEONG and Y.-S. JANG, *Compos. Struct.* **49** (2000) 443.
22. R. SEYDEL and F.-K. CHANG, *Smart Mater. Struct.* **10** (2001) 354.
23. R. SEYDEL and F.-K. CHANG, *ibid.* **10** (2001) 370.

Received 14 February 2002
and accepted 16 January 2003